Diabetes, Metabolic Syndrome and Obesity

Dovepress
Taylor & Francis Group

Open Access Full Text Article

ORIGINAL RESEARCH

Electroacupuncture Alleviates Oxidative Stress and Cuproptosis in Metabolic Dysfunction-Associated Steatotic Liver Disease Mice Through Activation of the NRF2/ARE Pathway

Junyuan Deng[1], Cai Liao[1], Hejing Liu[1], Xin Tang[1], Yan Yang[1], Yunhao Yang[2], Xiao Guo[1], Shanshan Zhang[1], Kehan Xing[1], Mei Liao[1], Chenglin Tang[1]

[1]College of Traditional Chinese Medicine, Chongqing Medical University, Chongqing, People's Republic of China; [2]College of Acupuncture and Tuina, Chongqing University of Chinese Medicine, Chongqing, People's Republic of China

Correspondence: Chenglin Tang, Email tangchenglin@cqmu.edu.cn

Purpose: Oxidative stress and the newly characterized mode of regulated cell death, cuproptosis, drive the progression of metabolic dysfunction-associated steatotic liver disease (MASLD). Electroacupuncture (EA) is a promising non-drug treatment, but its mechanisms are unclear. This study investigated the benefits of EA in a high-fat diet (HFD)-induced MASLD mouse model, focusing on the NRF2/ARE pathway, cuproptosis, and the gut–liver axis.

Methods: MASLD was established in C57BL/6J mice via a 16-week HFD. Mice were arbitrarily categorized into four groups: control (C, normal chow diet), model (M, HFD), EA (HFD + EA), and EA plus NRF2 inhibitor (EM, HFD + EA + inhibitor). A 4-week intervention was then conducted. Post-intervention, body weight alterations were tracked, and serum, liver tissue, and fecal specimens were gathered for subsequent examination.

Results: EA treatment significantly improved the metabolic profile, reducing body weight, lipids, and hepatic inflammation. It attenuated oxidative stress by enhancing antioxidant capacity and activated the NRF2/ARE pathway. EA also modulated cuproptosis-related genes (upregulating dihydrolipoamide S-acetyltransferase (Dlat), downregulating solute carrier family 31 member 1 (Slc31a1), ferredoxin reductase (Fdx1), and heat shock protein 70 (Hsp70)). Furthermore, EA remodeled the gut microbiota (increasing Limosilactobacillusand Ligilactobacillus) and elevated related metabolites.

Conclusion: EA ameliorates MASLD through multiple mechanisms, including regulating lipid metabolism, attenuating inflammation and oxidative stress, activating NRF2, suppressing cuproptosis, and altering the gut–liver axis, collectively contributing to hepatic improvement.

Keywords: gut microbiota, metabolomics, hepatic lipid metabolism, inflammation, mitochondrial dysfunction, antioxidant therapy

Introduction

A significant global health concern, metabolic dysfunction-associated steatotic liver disease (MASLD) ranks among the most common chronic liver conditions globally. Its prevalence has significantly increased in recent decades.[1] Recent epidemiological investigations estimate that MASLD affects more than three billion people worldwide,[2] underscoring its status as the predominant long-term liver disorder and emphasizing its substantial burden on healthcare systems. MASLD covers a wide range of clinical conditions, including nonalcoholic steatohepatitis, which can progress to severe liver fibrosis, cirrhosis, and hepatocellular carcinoma.[3–5] Cuproptosis represents a newly identified class of copper-mediated regulated cellular apoptosis, characterized by intracellular accumulation of excess copper ions, destabilization of iron–

https://doi.org/10.2147/DMSO.S568066
Received: 9 October 2025
Accepted: 29 December 2025
Published: 6 January 2026

Graphical Abstract

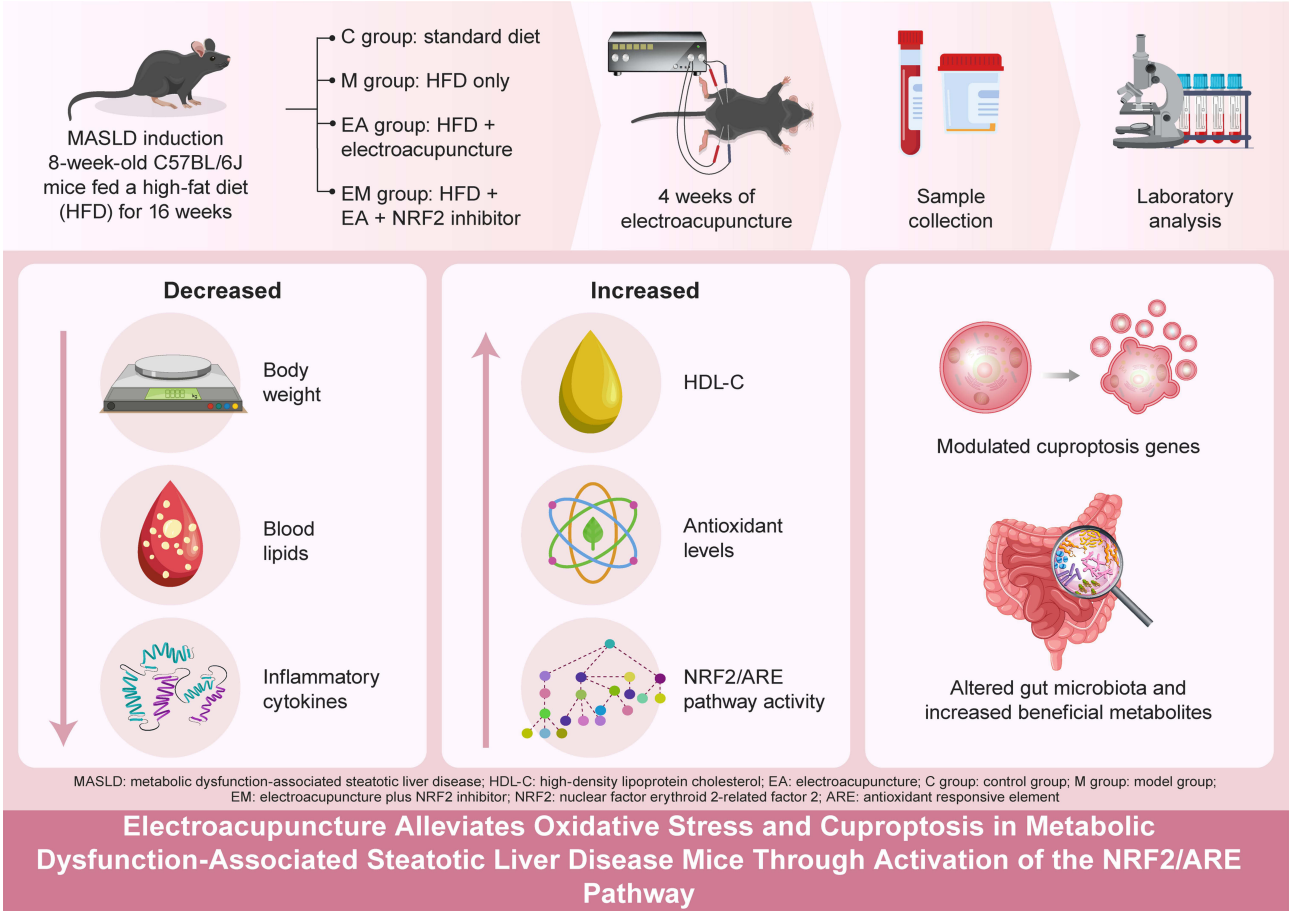

sulfur cluster proteins, and abnormal aggregation of lipoylated mitochondrial proteins.[6–8] The molecular execution of this process involves key genes, including the high-affinity copper importer SLC31A1, and the lipoylated components of the pyruvate dehydrogenase complex, which supplies acetyl-CoA for the tricarboxylic acid (TCA) cycle. An example is dihydrolipoamide S-acetyltransferase (DLAT). Also involved are ferredoxin reductase (FDX1), which is essential for iron–sulfur cluster biogenesis, and the stress-response molecular chaperone HSP70.[6–8] Unlike the well-characterized processes of apoptosis (a programmed cell death) and ferroptosis (an iron-dependent form of death driven by lipid peroxidation), cuproptosis is uniquely triggered by excessive copper and involves direct aggregation of mitochondrial proteins.[6–8] In the progression of MASLD, dysregulated copper metabolism leads to abnormal Cu^{2}+ accumulation, catalyzing excessive reactive oxygen species production via the Fenton reaction and thereby aggravating oxidative stress and hepatocyte injury.[9,10] Furthermore, copper ions can irreversibly bind to key lipoylated enzymes, such as pyruvate dehydrogenase and α-ketoglutarate dehydrogenase, inducing mitochondrial proteotoxic stress, respiratory chain dysfunction, and energy metabolism failure, ultimately impairing reactive oxygen species clearance and promoting cell death.[7,11,12] Electroacupuncture (EA) combines traditional acupuncture with contemporary electrical stimulation, involving the insertion of fine needles at specific acupoints followed by the application of a controlled, low-intensity electrical current. This approach provides sustained and regulated stimulation that integrates both electrophysiological and acupuncture effects.[13,14] Current clinical guidelines recommend lifestyle interventions as the first-line therapeutic strategy; however, weight loss alone does not always result in histological improvement.[15] Although vitamin E and pioglitazone have exhibited efficacy in randomized controlled trials, concerns remain regarding their long-term safety

and effectiveness.[16,17] Thus, developing novel, safe, and effective treatment strategies is crucial for MASLD management.

In recent years, EA has been widely investigated in both basic and clinical research on metabolic disorders. Critically, a growing number of clinical trials have demonstrated that EA intervention is safe and can significantly improve liver enzyme levels and hepatic steatosis in patients with MASLD.[18] This favorable safety profile supports its therapeutic potential.[19,20] Multiple studies have suggested that EA may benefit MASLD by reducing hepatic oxidative stress, regulating lipid metabolism, and suppressing inflammation.[20] Furthermore, the gut–liver axis, a bidirectional communication system between the gut microbiota, their metabolites, and the liver, is increasingly recognized as a critical player in MASLD pathogenesis.[21] However, whether EA improves MASLD through modulation of cuproptosis and the resulting impact on this gut microbiota–metabolite axis remains unclear, and the integrated molecular pathways through which EA ameliorates hepatic metabolic dysregulation and hepatocyte death have not been fully explained.

Therefore, the purpose of this research was to examine the curative effects and underlying mechanisms of EA in a high-fat diet (HFD)-induced MASLD mouse model, with a specific focus on whether EA alleviates hepatic lipid accumulation, inflammation, and oxidative stress. We aimed to determine whether EA delays MASLD progression by activating the NRF2/ARE antioxidant signaling pathway, preventing cuproptosis, and coordinately modulating gut–liver axis function.

Materials and Methods

Animals

Adult male C57BL/6 mice, 8 weeks old and weighing between 18 and 20 g, were supplied by the Laboratory Animal Center at Chongqing Medical University (Chongqing, China; SYXK [Yu] 20220010). The animals had unlimited access to food and water and were housed in a pathogen-free environment. The Chongqing Medical University Animal Ethics Committee approved all animal-related procedures (IACUC-CQMU-2024-0215). The procedure adhered to the American Veterinary Medical Association's guidelines on animal euthanasia. The mice were rendered unconscious through intraperitoneal injection of sodium pentobarbital (150 mg/kg). Following confirmation of deep sedation based on the absence of pedal reflexes, swift cervical dislocation was executed as an additional physical means to guarantee a humane end. This study has been reported in accordance with the ARRIVE (Animal Research: Reporting of in vivo Experiments) Guidelines.

After a one-week acclimation period, mice were divided into two cohorts: a control group (C, n = 10) fed normal chow (15.91% fat calories) and an experimental cohort (n = 35) fed a high-fat diet (HFD, 60% fat calories) for 16 weeks to induce non-alcoholic fatty liver disease. Successful induction was confirmed by histological assessment of liver tissues from five randomly selected mice. Following confirmation, the remaining mice (n = 30) were randomly assigned to three experimental groups using a random number table to minimize bias:the model group (M, n = 10, continued HFD), the electroacupuncture group (EA, n = 10, HFD + electroacupuncture), and the combination group (EM, n = 10, HFD + electroacupuncture + the NRF2 inhibitor ML385 [30 $mg \cdot kg^{-1} \cdot day^{-1}$, intraperitoneal]). All interventions were administered once daily, six days per week for 4 weeks. Throughout the study, the C group remained on normal chow, while all other groups continued the HFD.

After treatment, we collected fecal samples and stored them at −80 °C. Prior to experimental procedures, all mice were fasted overnight and anesthetized with sodium pentobarbital. Under deep anesthesia, whole blood was collected via terminal cardiac puncture and immediately placed into coagulation-promoting tubes.After incubation at room temperature for 30 min, we centrifuged the samples at 4°C at 1200 × g for 20 min. The supernatant was carefully removed to obtain serum, which was then stored at −80°C. Livers were excised and weighed. Each liver sample was fixed with 4% paraformaldehyde for histological preservation. The tissue samples that remained were promptly frozen using liquid nitrogen at −80°C and retained for further analysis.

Electroacupuncture Intervention

In MASLD mouse models, prior research has demonstrated that stimulating the ST36 and ST40 acupoints provides therapeutic benefits.[22] According to anatomical references, ST36 (Zusanli) is located approximately 4 mm below the

knee joint, whereas ST40 (Fenglong) is located about 5 mm above the tip of the external malleolus. During treatment, mice were gently restrained using a holding device to maintain proper positioning. Target sites in the EA and EM groups were cleaned with 75% alcohol before needle insertion. Acupuncture needles (0.16 × 13 mm; Zhenzheng Medical Devices Co., Ltd., Xinyang, Henan, China) were inserted bilaterally at ST36 and ST40 to a depth of 2–3 mm. The needles were connected to an electroacupuncture machine delivering an amplitude-modulated 2/15 Hz stimulus at 0.5–1.0 mA. Mice in the EA group received daily 10-min treatments. The EM group underwent the same electroacupuncture procedure, followed by daily intraperitoneal injection of the NRF2 inhibitor ML385 at a dosage of 30.0 $mg \cdot kg^{-1} \cdot day^{-1}$. The control and model groups received no electrical stimulation or acupuncture but were placed in identical restraining devices for the same duration to control for handling effects.

Biochemical Analysis

Serum concentrations of triglyceride (TG), total cholesterol (TC), low-density lipoprotein cholesterol (LDL-C), high-density lipoprotein cholesterol (HDL-C), AST, and ALT were quantified with commercial assay kits (Jiancheng Bioengineering Institute, Nanjing, China).Hepatic levels of glutathione (GSH) (S0053), malondialdehyde (MDA) (S0131S), superoxide dismutase (SOD) (S0101S), and total antioxidant capacity (T-AOC) (S0121) were determined utilizing commercially available kits (Beyotime Biotechnology).

Enzyme-Linked Immunosorbent Assay Analysis

Serum concentrations of pro-inflammatory cytokines, such as IL-1β (JM-02323M1), IL-6 (JM-02446M1), and TNF-α (JM-02415M1), were measured using a commercially available murine enzyme-linked immunosorbent assay (ELISA) kit, following the manufacturer's instructions. Briefly, standards and samples were dispensed in duplicate into microwells pre-coated with capture antibody. Incubation and subsequent washing processes were followed by the addition of a biotin-conjugated detecting antibody. Streptavidin-HRP was then added, and the plate was incubated. Then, a substrate of tetramethylbenzidine was added to induce a colorimetric reaction. We stopped the reaction with sulfuric acid solution and then measured the absorbance at 450 nm. Cytokine levels are measured in picograms per milliliter (pg/mL) using a standard curve.

Transmission Electron Microscopy

TEM was performed to assess ultrastructural changes in hepatocyte mitochondria, including morphology, cristae structure, and signs of swelling or disruption, as indicators of cellular stress and injury.Briefly, liver specimens were fixed three times with 1% osmium tetroxide solution after being rinsed three times with 0.1 mol/L phosphate-buffered saline. Subsequently, samples were dehydrated using a graded series of ethanol and acetone solutions at 4 °C, with the final step completed in 100% acetone at room temperature. The dehydrated tissues were infiltrated with resin and then polymerized in an oven. Sections (70 nm thick) were prepared using an ultramicrotome. The sections were stained sequentially with 3% uranyl acetate and then with lead citrate to enhance contrast for observation under an electron microscope.

Histopathological Examination

Liver tissues from each mouse were fixed in 4% paraformaldehyde. The fixed tissues were then processed, embedded in paraffin blocks, and sectioned at 4 μm thickness. The sections were used for two staining protocols: (1) Hematoxylin and eosin (H&E) staining: H&E-stained sections were evaluated for general histopathology. The histopathological severity of steatohepatitis was assessed in a blinded manner by an experienced pathologist. A semi-quantitative scoring was performed using the modified Kleiner NAFLD activity score (NAS) system, which evaluates steatosis, lobular inflammation, and hepatocyte ballooning. A composite score (ranging from 0 to 8) was generated for each animal.[23] (2) Oil Red O (ORO) staining: Paraffin-embedded sections were also subjected to ORO staining for the visualization of neutral lipid droplets. It should be noted that, as the tissues were paraffin-embedded, the ORO staining in this study is interpreted primarily for qualitative assessment and within-study comparison of lipid droplet distribution under identical processing conditions, rather than for absolute quantitative analysis of neutral lipid content.All stained sections were examined and imaged under a light microscope.

Immunofluorescence Examination

After dewaxing, we performed antigen retrieval, membrane permeabilization, and sealing on paraffin-embedded liver tissue sections. The samples were then placed in a moist box and left to sit at room temperature for 1 h while being incubated with the main antibody. The antibodies used were Nrf2 (No. AF02883, AiFang) and HO-1 (No. A1346, Abclonal). After washing three times with phosphate-buffered saline, the sample was probed with the corresponding secondary antibody (Alexa Fluor® 488) (No. ab150113, Abcam) at 22–26 °C for 1 h. We used 4′,6-diamidino-2-phenylindole hydrochloride (No. D9542, Sigma-Aldrich) to visualize the nucleus and YF594-phalloidin (No. YP0052, US Everbright) to label the actin filaments. Every staining procedure was carried out in absolute darkness. Finally, images were captured using an inverted fluorescence microscope.

Quantitative Real-Time PCR

Total RNA was extracted from 50 mg of mouse liver using a SteadyPure Rapid RNA Extraction Kit (AG21023) according to the manufacturer's instructions. RNA was reverse-transcribed using the Evo M-MLV RT Mix Kit with gDNA Clean for qPCR (AG11728). Quantitative real-time PCR (qRT-PCR) was performed with the SYBR Green Pro Taq HS qPCR Kit (AG11701) on a Bio-Rad CFX Connect real-time PCR instrument. The qPCR was carried out in a 20 μL reaction mixture containing 10 μL of 2× SYBR Green Pro Taq HS Premix, 0.4 μL each of forward and reverse primer (10 μM), 0.4 μL of ROX Reference Dye, 2 μL of cDNA template, and 6.8 μL of nuclease-free water. The thermocycling conditions were as follows: initial denaturation at 95°C for 30 seconds; followed by 40 cycles of 95°C for 5 seconds and 60°C for 30 seconds; with a final melt curve analysis step. Relative quantification was calculated utilizing the $2^{-\Delta\Delta Ct}$ method after normalization to β-ACTIN. Table 1 lists the primers used for qRT-PCR.

Western Blotting Analysis

Protein expression was evaluated through Western blotting. Tissue samples were homogenized and lysed in RIPA buffer to extract total protein. Equal quantities of protein in the lysates were resolved using polyvinylidene fluoride membranes after separation via SDS-PAGE. Unconjugated primary antibodies were used to probe the membranes overnight at 4 °C against: Nrf2 (1:500,AiFang, AF02883), HO-1 (1:500,AF11846, AiFang), DLAT (1:10000,12346-1-AP, Proteintech), FDX1 (1:1000,12592-1-AP, Proteintech), NQO1 (1:5000,67240-1-lg, Proteintech), SLC31A1 (1:500,27499-1-AP, Proteintech), and HSP70 (1:10000,10995-1-AP, Proteintech). β-ACTIN (1:10000,EM21002, HUABIO) served as the internal control. Immunoreactive bands were found using a chemiluminescence imaging device (Image Studio), and ImageJ software was used to quantify the band intensities.

Fecal Microbiota Analysis

Bacterial DNA was extracted from frozen stool samples. The V3-V4 region of the 16S rRNA gene was PCR-amplified using barcoded specific primers. Sequencing libraries were prepared with the TruSeq Nano DNA LT Library Prep Kit. PCR amplification was performed with Phusion High-Fidelity PCR Master Mix with GC Buffer under standard cycling conditions. Sequencing was conducted on a NovaSeq 6000 platform using paired-end reads.

Table 1 Sequences and Product Length of Primers Used

Gene	Forward Primer	Reverse Primer
SLC31A1	GCACATCATCCAGGTAGTCATCA	CCACCACTGCCTTCTTCCA
HSP70	CAGTAGCCTGGGAAGACATATAGT	GTAGTACACAGTGCCAAGACG
DLAT	TTAGCCTCCAAAGCGAGAGAG	TCTGAAGCACCGATTGCCAG
FDX1	CAAGAACCGAGATGGCGAGA	GTAGAGCAAGCCAACGTTCC

https://doi.org/10.2147/DMSO.S568066

Non-Targeted Metabolomics

After aggressively mixing the mouse fecal samples with a 2-chlorophenylalanine methanol solution, the mixture was centrifuged at 15,000 rpm and 4 °C for 15 min. The supernatant was analyzed through UPLC-MS using a Waters ACQUITY system fitted with an HSS T3 column (2.1 × 100 mm, 1.8 μm) at 40 °C with a flow rate of 0.3 mL/min. A Thermo Q Exactive apparatus was used to perform mass spectrometry. The top three ions were subjected to data-dependent MS^2 fragmentation (30 eV) at 17,500 resolution after full MS scans (m/z 100–1000) were obtained at 70,000 resolution. Redundancy was decreased using dynamic exclusion.

Statistical Analyses

We used GraphPad Prism 9 (GraphPad Software, San Diego, CA, USA) for statistical analysis. All datasets were confirmed to follow a normal distribution using normality tests. The data are displayed as the mean ± standard deviation (SD). A one-way analysis of variance (ANOVA) was used for comparisons between three or more groups. When the ANOVA indicated a significant difference ($p < 0.05$), Tukey's honestly significant difference (HSD) post-hoc test was applied for all pairwise comparisons.The threshold for significance was $p < 0.05$.

Results

EA Attenuates Obesity-Related Features in HFD-Induced MASLD Mice

Mice fed a HFD gained more weight than those in the control group (Figure 1A). EA intervention significantly reduced HFD-induced weight gain and fat accumulation and improved dyslipidemia. Specifically, the M group showed significantly raised serum concentrations of TC, TG, and LDL-C, along with diminished HDL-C concentrations, relative to the C group. In contrast, EA therapy significantly lowered TC, TG, and LDL-C while increasing HDL-C (Figure 1B–F). These findings indicate that EA effectively reduced lipid metabolic disturbances and obesity induced by HFD.

EA Ameliorates Hepatic Steatosis in MASLD Mice

Hepatic lipid accumulation, as visualized by H&E and Oil Red O staining, was markedly increased in the model (M) group compared to the control (C) group, characterized by variably sized lipid vacuoles and disordered hepatocellular arrangement (Figure 2A and B). EA treatment significantly reduced lipid accumulation and improved hepatic steatosis (Figure 2B and D). To quantify the histopathological severity, liver sections were evaluated using the NAFLD Activity Score (NAS) system. The composite NAS was significantly higher in the M group than in the C group, and EA treatment significantly attenuated this increase (Figure 2C).Consistent with these morphological findings, serum ALT and AST levels, as determined by ELISA, were substantially elevated in the M group compared to the C group. EA intervention considerably reduced both ALT and AST levels. Interestingly, the ALT and AST concentrations in the EM group (EA + NRF2 inhibitor) were noticeably higher than those in the EA group (Figure 2E and F).

EA Attenuates Hepatic Inflammation and Oxidative Stress in MASLD Mice

Transmission electron microscopy analysis of hepatic mitochondrial ultrastructure revealed largely normal morphology in the C group, with intact outer and inner membranes, no membrane rupture or abnormal fusion, and regularly arranged cristae without swelling, vacuolation, or density alterations. In contrast, the M group exhibited pronounced mitochondrial abnormalities, including swelling and fragmentation, largely attributable to compression by lipid droplets. The EA group demonstrated a discernible reduction in mitochondrial damage compared with the M group (Figure 3A). ELISA results indicated higher TNF-α, IL-6, and IL-1β serum levels in the M group than in the C group (Figure 3B–D). EA treatment considerably decreased these pro-inflammatory cytokine levels compared with the M group. Hepatic oxidative stress indicators were significantly different between the M and C groups, showing reduced GSH, T-AOC, and SOD concentrations and increased MDA concentrations. EA intervention effectively reversed these changes, increasing GSH, T-AOC, and SOD and decreasing MDA levels. Notably, the EM group exhibited significantly lower GSH, T-AOC, and SOD and higher MDA concentrations than in the EA group (Figure 3E–H).

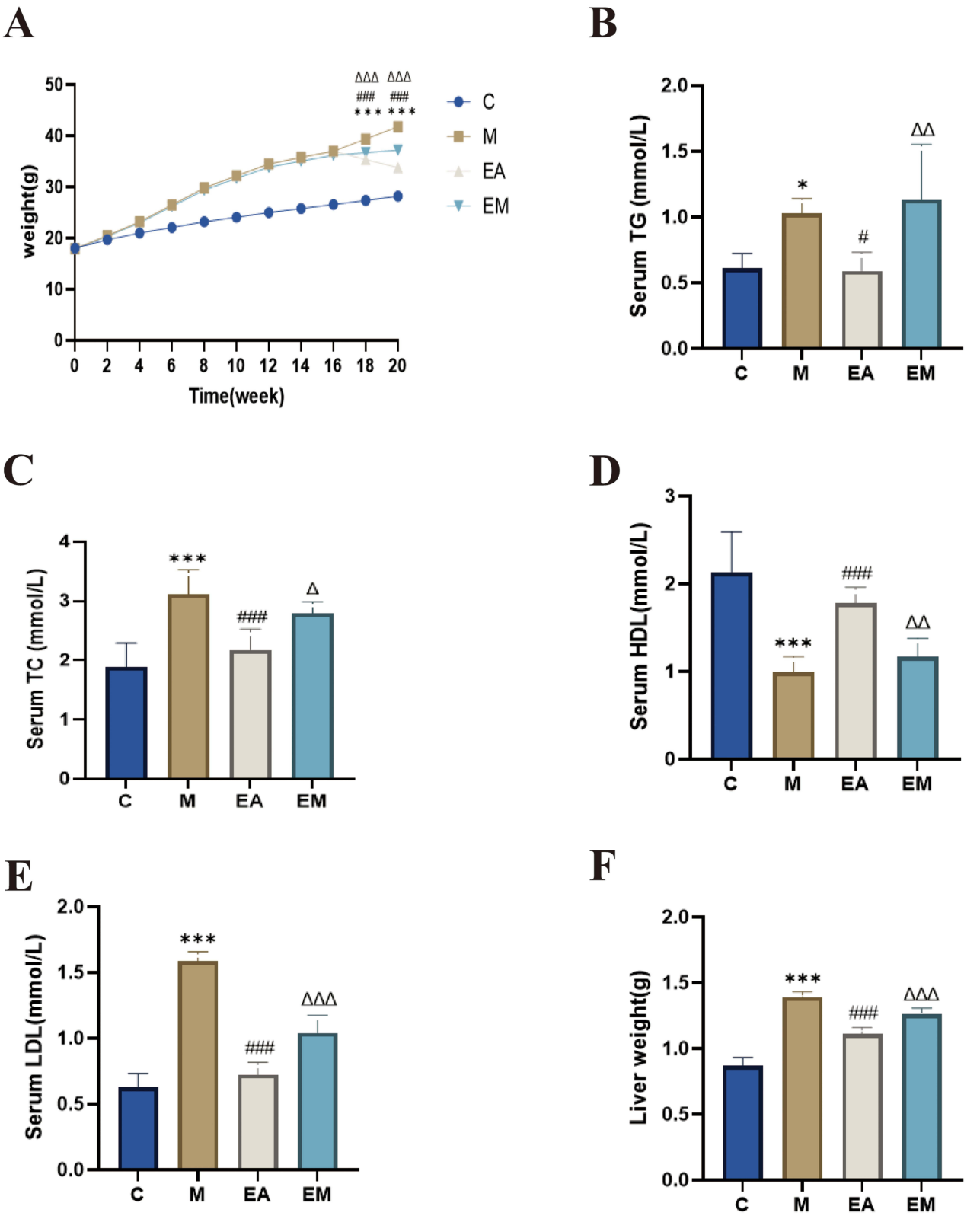

Figure 1 EA decreased hepatic fat accumulation and body weight. (**A**) Gain in body weight; (**B**) serum TG; (**C**) serum TC; (**D**) serum HDL; (**E**) serum LDL; (**F**) liver weight. n = 6, values are mean ± SD; *p < 0.05,***p < 0.001 (C vs M); #p < 0.05, ###p < 0.001 (M vs EA); Δp < 0.05, ΔΔ p < 0.01, ΔΔΔp < 0.001 (EA vs EM).

https://doi.org/10.2147/DMSO.S568066

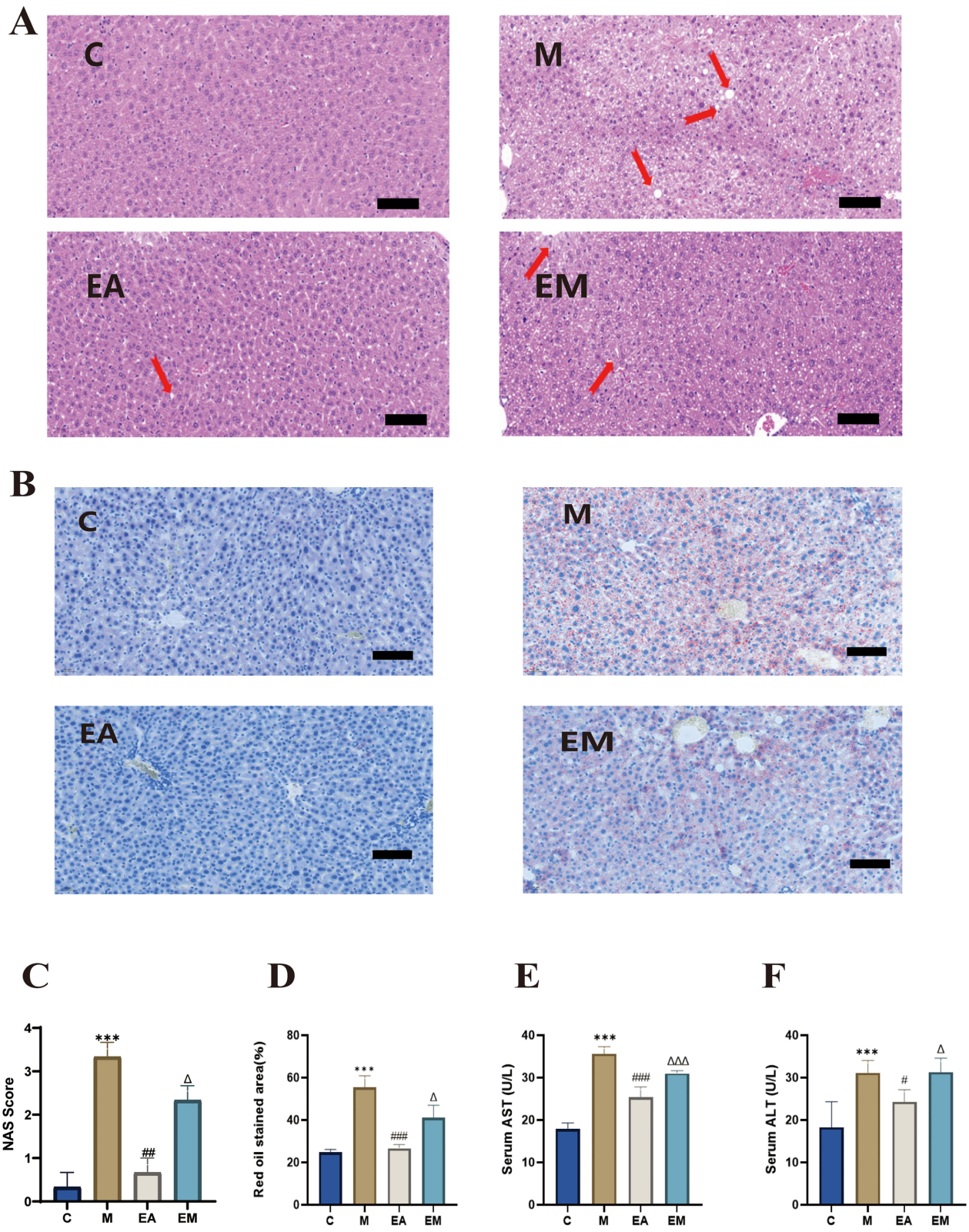

Figure 2 EA ameliorates hepatic steatosis and enhances liver function in mice. (**A**) Sample liver slices stained with H&E (scale bar = 100 μm). Red arrows indicate inflammatory cell infiltration; (**B**) Liver slices stained with Oil Red O (scale bar = 100 μm); (**C**) NAFLD Activity Score (NAS); (**D**) Quantification of Oil Red O-positive areas (%); (**E**) Serum AST levels; (**F**) Serum ALT levels. For all data panels in this figure, n = 6 mice per group, aside from the NAFLD Activity Score (NAS) and quantification of Oil Red O-positive areas (%), where n = 3, values are mean ± SD;***p < 0.001 (C vs M); #p < 0.05, ##p < 0.01,###p < 0.001 (M vs EA); Δp < 0.05, ΔΔΔp < 0.001 (EA vs EM).

https://doi.org/10.2147/DMSO.S568066

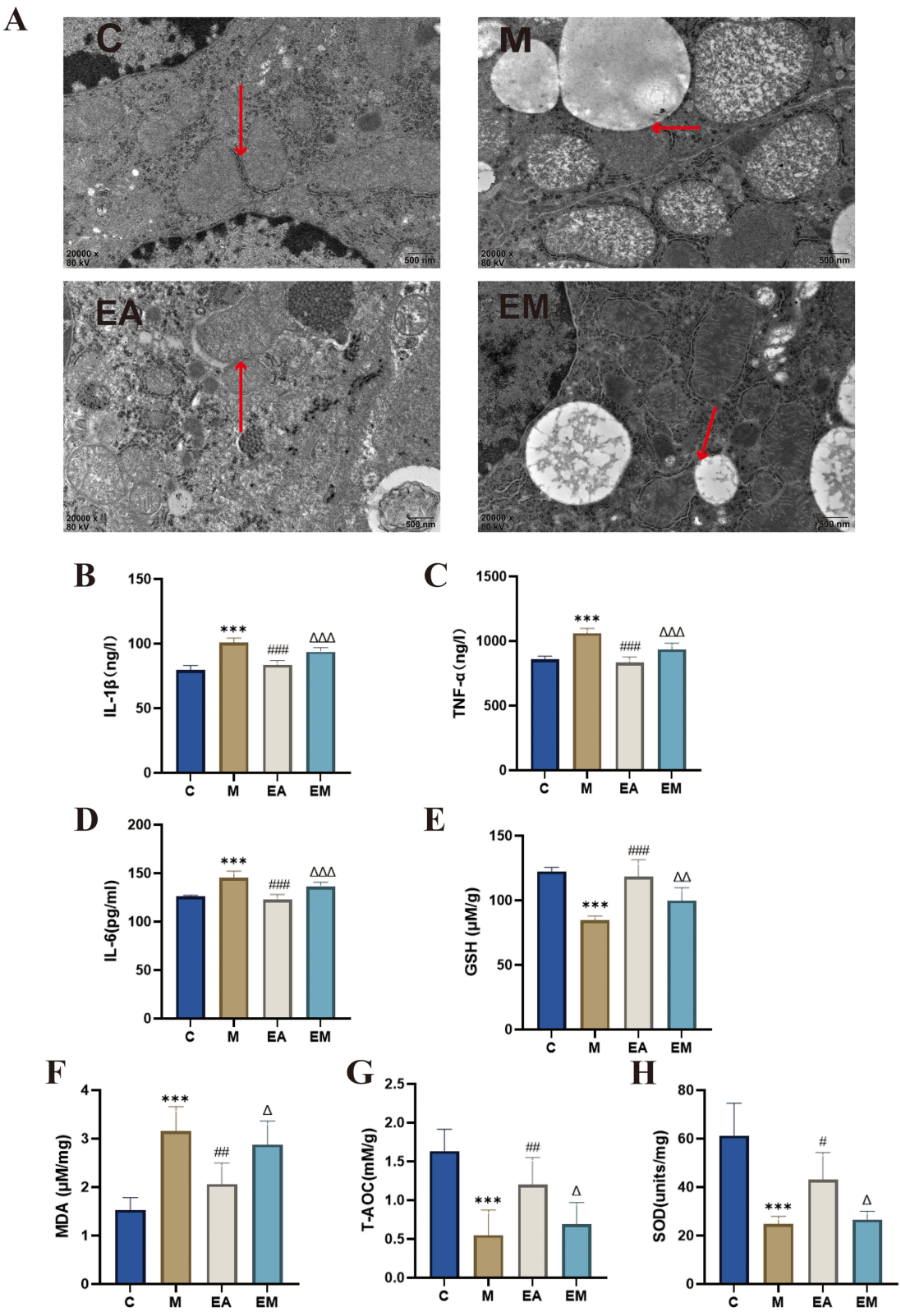

Figure 3 EA mitigates inflammation and ameliorates oxidative stress in mice. (**A**) Representative electron micrographs of hepatic mitochondria (scale bar = 500 μm). Red arrows indicate mitochondrial membrane structures; (**B**) hepatic IL-1β levels; (**C**) hepatic TNF-α levels; (**D**) hepatic IL-6 levels; (**E**) hepatic GSH levels; (**F**) hepatic MDA levels; (**G**) hepatic T-AOC; (**H**) hepatic SOD levels. n = 6, values are mean ± SD;***p < 0.001 (C vs M); #p < 0.05, ##p < 0.01, ###p < 0.001 (M vs EA); Δp < 0.05, ΔΔp < 0.01, ΔΔΔp < 0.001 (EA vs EM).

https://doi.org/10.2147/DMSO.S568066

Metabolomic Analysis Reveals Targets and Pathways of EA Intervention in MASLD

Fecal samples were subjected to untargeted metabolomics to further investigate metabolic pathway changes linked to EA intervention in MASLD. Principal component analysis and OPLS-DA revealed distinct metabolic profiles in the C, M, and EA groups (Figure 4A–E). Using thresholds of VIP > 1 and $p < 0.05$, 1118 differential metabolites were identified between the C and M groups, and 1307 between the EA and M groups (Figure 4F). KEGG enrichment analysis indicated significant involvement of oxidative stress-related pathways, including central carbon metabolism in cancer, renal cell carcinoma, breast cancer, alanine–aspartate–glutamate metabolism, and the TGF-β signaling pathway (Figure 4G).Central carbon metabolism in cancer was selected for further investigation. EA intervention significantly upregulated four key metabolites in this pathway: l-cysteine (AUC = 0.944), l-glutamic acid (AUC = 1), succinic acid (AUC = 1), and citric acid (AUC = 1). Compared with the M group, EA treatment markedly increased levels of these metabolites ($p < 0.01$) (Figure 4H–P). These results suggest that EA may alleviate MASLD by modulating critical metabolic pathways, particularly central carbon metabolism, thereby enhancing antioxidant responses and supporting its therapeutic potential.

Effect of EA Administration on the NRF2/ARE Signaling Pathway in Mice with HFD-Induced MASLD

Immunofluorescence analysis showed that liver tissues from the M group had considerably lower fluorescence intensities of NRF2 and HO-1 compared with those from the C group, indicating inhibition of the NRF2/ARE signaling pathway. In contrast, the EA group exhibited markedly stronger fluorescence signals for both NRF2 and HO-1 than either the M or EM groups, indicating that EA promoted NRF2 pathway activation (Figure 5A). These results were consistent with findings from Western blot analysis (Figure 5B–E).

EA Inhibits Cuproptosis in HFD-Induced MASLD Mice

To elucidate the mechanism by which EA treats HFD-induced MASLD, we examined cuproptosis. Key markers of cuproptosis include HSP70, DLAT, FDX1, and SLC31A1. Compared with the control group, the HFD group exhibited significantly decreased DLAT expression, which was restored by EA intervention. In addition, the EA group exhibited reduced hepatic expression of HSP70, FDX1, and SLC31A1 compared with the M group. EA treatment further decreased these markers relative to the EM treatment (Figure 6A–I). Collectively, these results suggest that EA may inhibit cuproptosis via activation of the NRF2/ARE signaling pathway, contributing to its therapeutic effect in MASLD.

Impact of EA on the Gut Microbiota in MASLD Caused by an HFD

To investigate how EA intervention affects the gut microbial community in MASLD mice, a PCoA was carried out based on OTU abundance data from the C, M, and EA groups. The PCoA plot revealed that the microbial community structure of the EA group was similar to that of the C group, whereas a clear spatial separation was noted between the M and EA groups, indicating that EA markedly altered the gut microbiota composition in HFD-induced MASLD mice (Figure 7A and B). Differential species analysis demonstrated that 425 ASVs/OTUs were shared between the EA and M groups. A total of 1219 OTUs were identified in the M group, whereas EA treatment increased the number of OTUs to 3333, suggesting a significant enhancement in microbial richness following EA intervention (Figure 7C). To delve deeper into the taxonomic distribution of organisms in various regions, the prevalence of ASVs/OTUs was assessed at the phylum and genus taxonomic ranks (Figure 7D). EA significantly increased the proportion of Limosilactobacillus ($p < 0.001$) and Ligilactobacillus ($p < 0.05$) (Figure 7E and F). Additionally, in a co-occurrence network analysis of the top 50 most abundant species, the microbial community clustered into five major functional groups (Figure 7G). In summary, EA may exert its therapeutic effects in MASLD partly by remodeling the gut microbiota composition, particularly by enriching key beneficial genera, such as Limosilactobacillus and Ligilactobacillus, thereby providing mechanistic insights into its role in mitigating MASLD.

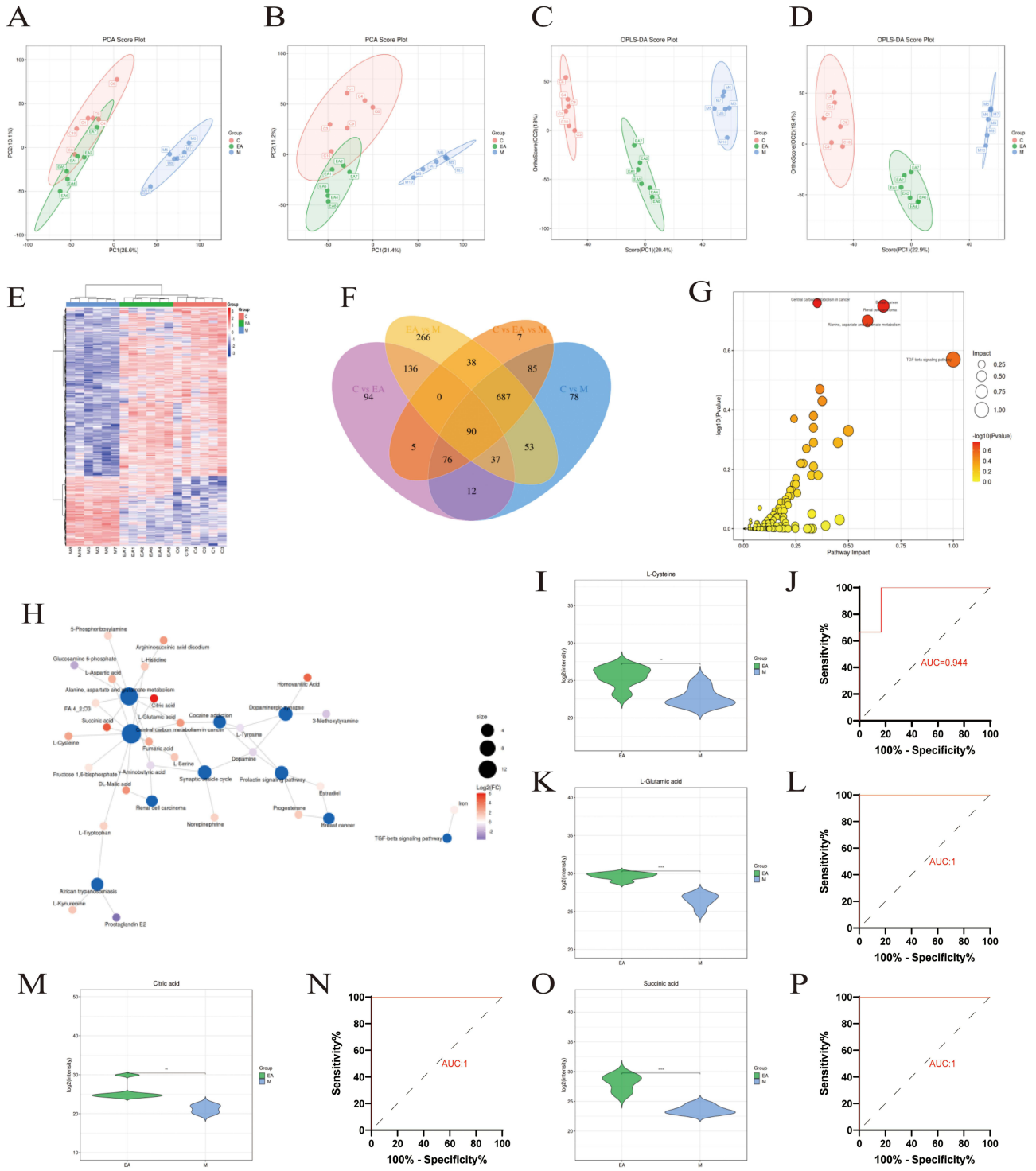

Figure 4 Effect of EA on fecal untargeted metabolomics in high-fat diet-fed mice. (**A** and **B**) Principal component analysis (PCA) plots for positive and negative ions; (**C, D**) OPLS-DA score plots comparing M and EA groups in negative- and positive-ion modes, respectively; (**E**) heat map of overall metabolite clustering; color intensity indicates relative abundance, with blue denoting lower expression and red denoting higher expression. Columns represent samples, rows represent metabolites, and the dendrogram on the left shows metabolite clustering. (**F**) Differentially abundant metabolites. (**G**) Scatter plot of pathway impact analysis: x-axis represents impact value of enriched metabolic pathways, y-axis shows $-\log_{10}$(P value);darker hues indicate lower P values. (**H**) Network diagram of differential metabolites between EA and M groups; blue nodes represent pathways, other nodes denote metabolites, with larger and darker nodes indicating greater differential abundance. (**I, K, M** and **O**) Quantitative results for selected metabolites; (**J, L, N** and **P**) Related metabolite ROC analyses. n = 6, values are mean ± SD; *p < 0.05, **p < 0.01, ***p < 0.001 (M vs EA).

https://doi.org/10.2147/DMSO.S568066

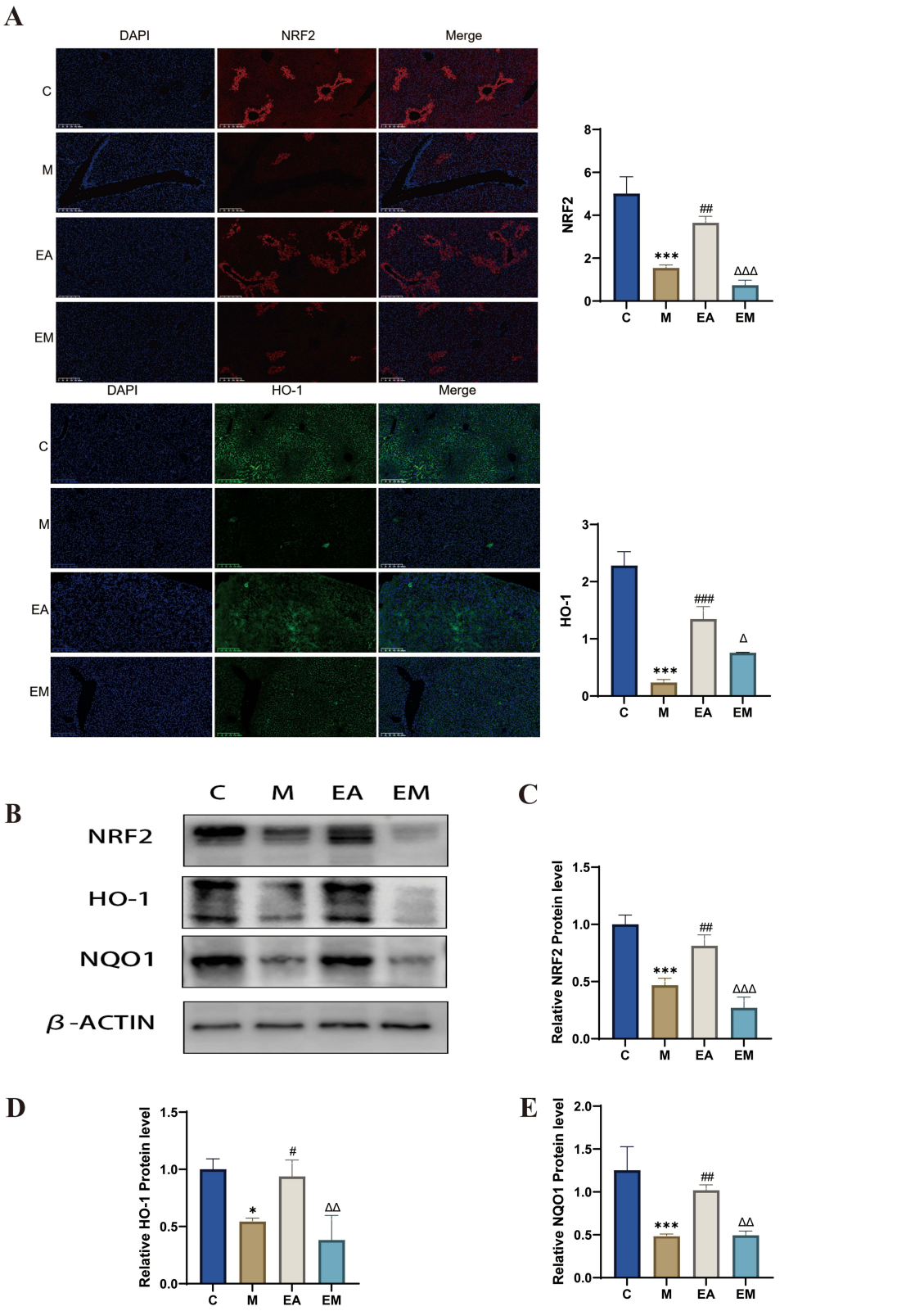

Figure 5 Impact of EA on hepatic NRF2/ARE signaling pathways. (**A**) Immunofluorescence of liver tissue (scale bar = 200 μm). (**B**–**E**) Immunoblot analysis of individual protein expression (β-actin as internal reference). n = 3, values are mean ± SD;*p < 0.05, ***p < 0.001 (C vs M); #p < 0.05, ## p < 0.01, ###p < 0.001 (M vs EA); Δ p < 0.05, ΔΔ p < 0.01, ΔΔΔ p < 0.001 (EA vs EM).

https://doi.org/10.2147/DMSO.S568066

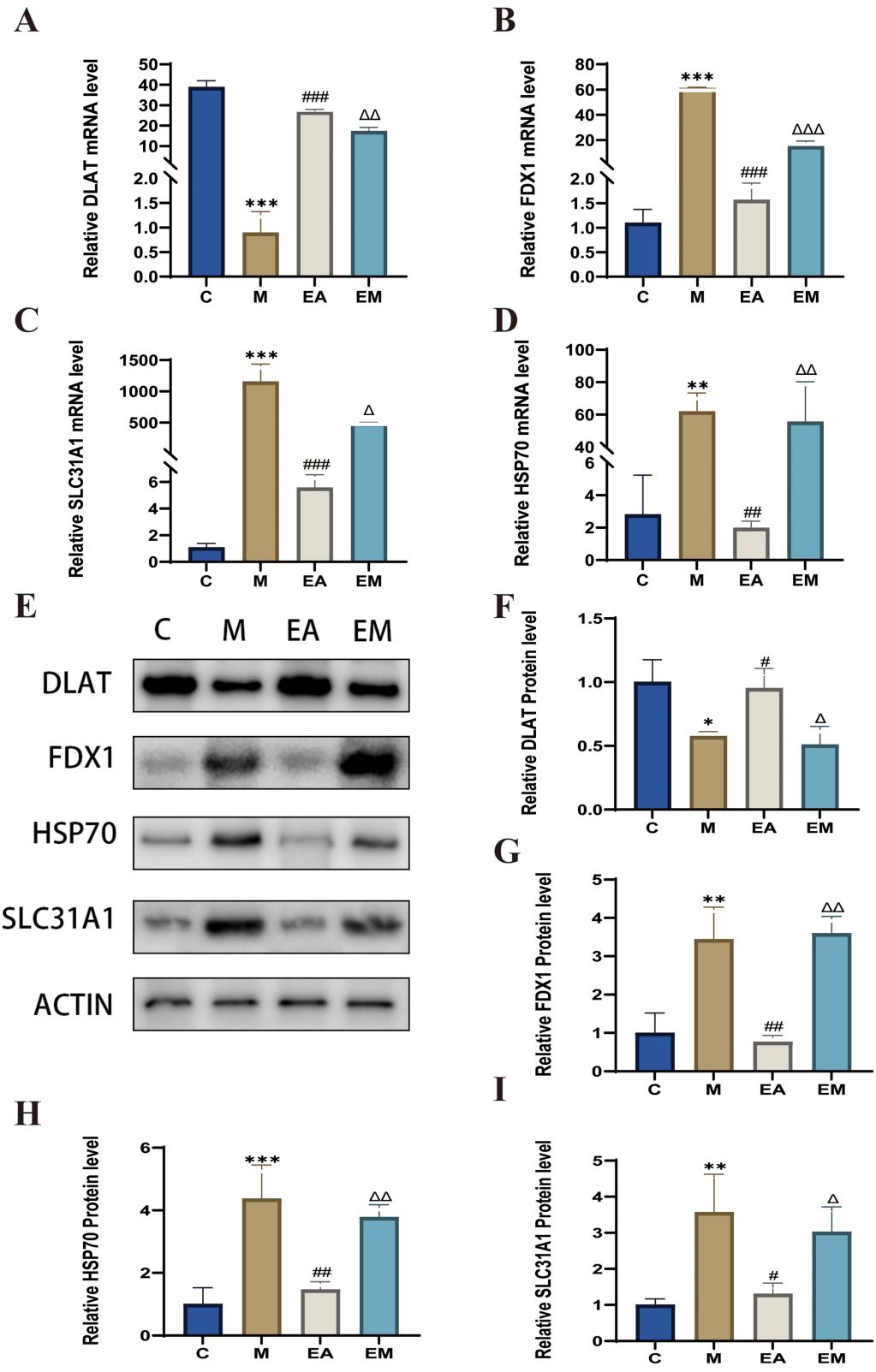

Figure 6 EA ameliorates MASLD by suppressing hepatic cuproptosis: insights from gene and protein expression analyses. (**A**–**D**) Gene expression (β-actin as internal reference). (**E**–**I**) Protein expression (β-actin as internal reference). n = 3, values are mean ± SD; *p < 0.05, **p < 0.01,*** p < 0.001 (C vs M); #p < 0.05, ## p < 0.01, ###p < 0.001 (M vs EA); Δ p < 0.05, ΔΔ p < 0.01, ΔΔΔ p < 0.001 (EA vs EM).

https://doi.org/10.2147/DMSO.S568066

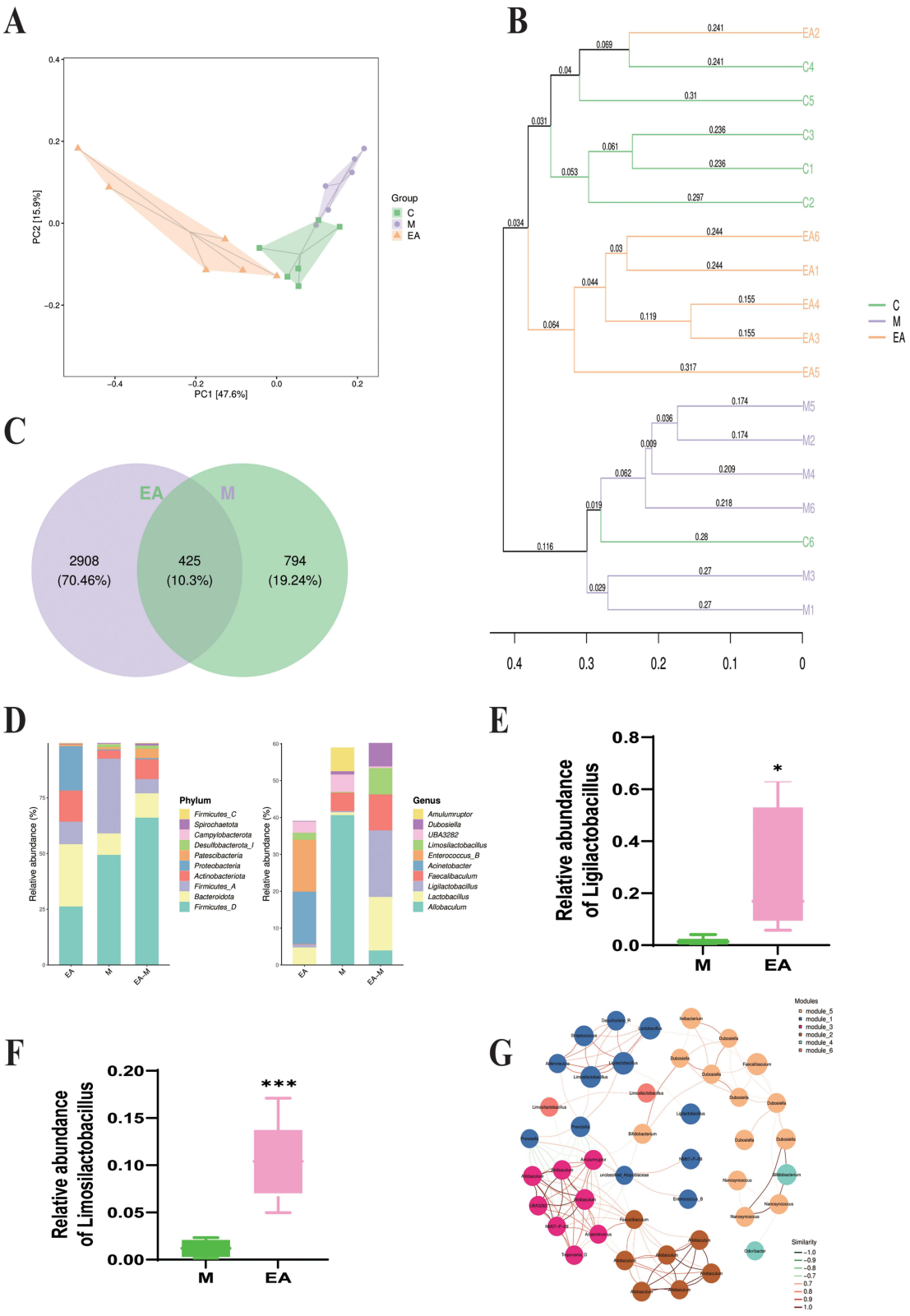

Figure 7 Effect of EA on gut microbiota in high-fat diet-fed mice. (**A**) Principal coordinate analysis (PCoA); each point represents a sample, colors indicate distinct groups; (**B**) UPGMA cluster analysis; (**C**) Venn diagram showing overlap of amplicon sequence variants/operational taxonomic units (ASVs/OTUs) among groups; (**D**) bar plots showing ASV/OTU abundance in distinct regions of the Venn diagram; (**E** and **F**) changes in relative abundances of Limosilactobacillus and Ligilactobacillus; (**G**) co-occurrence network of dominant microbial species. Each node represents an ASV/OTU, with node size proportional to abundance (log_2(CPM/n)). Only the 50 most abundant ASVs/OTUs are shown. Modules are color-coded to represent the top 10 most-connected clusters. n = 6, values are mean ± SD; *p < 0.05, ***p < 0.001 (M vs EA).

https://doi.org/10.2147/DMSO.S568066

Discussion

Currently, there are no universally approved pharmacological treatments for MASLD.[24] Common drug-based approaches primarily target a single or limited number of pathological mechanisms, such as insulin sensitizers (eg pioglitazone),[25] antioxidants (eg vitamin E),[26] and lipid-lowering agents.[27] In contrast, EA has been reported to ameliorate MASLD through multiple synergistic mechanisms while maintaining a favorable safety profile with minimal adverse effects.[20,28] The therapeutic benefits of EA on MASLD and the underlying mechanisms were examined in this study. Our findings demonstrate that, by suppressing cuproptosis, modulating the gut microbiota–metabolite axis, and activating the NRF2 antioxidant pathway, EA intervention substantially reduces MASLD and associated metabolic disturbances.

In this study, EA intervention significantly ameliorated histopathological liver damage in a mouse model of MASLD. Mechanistically, the hepatic levels of important pro-inflammatory cytokines, such as IL-6, TNF-α, and IL-1β, were significantly decreased after EA therapy, suggesting that local inflammatory responses were effectively suppressed. Concurrently, EA alleviated oxidative stress, as evidenced by increased SOD activity and elevated T-AOC and GSH levels, together with reduced levels of MDA, a marker of lipid peroxidation. At the metabolic level, EA effectively modulated systemic metabolic phenotypes, leading to significant decreases in body weight and fat storage. It also induced favorable changes in serum lipid profiles, characterized by decreased atherogenic lipid levels of TG, TC, and LDL-C and increased HDL-C. In summary, our findings suggest that EA exerts multidimensional protective effects by improving lipid metabolism, reducing obesity, and mitigating liver damage by modulating inflammation, oxidative stress, and metabolic homeostasis. These preclinical results provide a solid mechanistic foundation for the clinical translation of EA. They indicate that future clinical trials can focus on verifying whether EA can activate the NRF2 pathway and inhibit cuproptosis in MASLD patients, and explore its potential as an adjunctive therapy to complement existing lifestyle interventions and pharmacological treatments, particularly for patients with inadequate responses to conventional therapies.These results validate the application of EA as a promising non-pharmacological intervention with integrated benefits for MASLD management.[19]

Cuproptosis is dependent on mitochondrial respiration and is activated by excessive copper ions.[29,30] We discovered that the expression of important genes linked to cuproptosis, such as Slc31a1, Fdx1, and Hsp70, was markedly downregulated by EA therapy. Additionally, EA therapy increased Dlat expression. Slc31a1 encodes a copper transporter protein, and its reduced expression may limit cellular copper uptake.[31] FDX1, which reduces Cu^{2}+ to the more toxic Cu+, functions as a central regulator of cuproptosis.[32] Excess copper ions attach to DLAT's lipoylation sites during cuproptosis, causing it to oligomerize. As a result, the protein loses its function and aggregates toxically. Concurrently, the cellular response to such proteotoxic stress is the upregulation of Hsp70.[33] These alterations in gene expression suggest that EA intervention may protect cellular metabolic function by suppressing the cuproptosis pathway, which could represent a key cellular mechanism underlying its beneficial effects on systemic energy metabolism and lipid homeostasis.

Cuproptosis, A a unique kindform of cell death called cuproptosis is dependent on mitochondrial respiration and, is brought oninduced by excessive copper ions.[29,30] We discoveredobserved that the manifestation of important genes linked to cuproptosis, such as SLC31A1, FDX1, and HSP70, was EA therapy markedly downregulated the expression of key cuproptosis-related genes, including SLC31A1, FDX1, and HSP70 by EA therapy. Additionally, while EA therapy increasinged DLAT expression. SLC31A1 encodes a copper transporter protein, and its reduced expression may limit cellular copper uptake.[31] FDX1, which reduces Cu^{2}+ to the more toxic Cu+, functions as a central regulator of cuproptosis.[32] During cuproptosis, excess copper ions attachbind to DLAT's lipoylation sites during cuproptosis, causing it to oligomerationize. As a result, the protein loses its functional loss, and toxic aggregationes toxically. Concurrently, the cellular response to such proteotoxic stress involves an up-regulation of HSP70 expression.[33] These alterations in gene expression changes suggest that EA intervention may protect cellular metabolic function by suppressing the cuproptosis pathway, which could representing a key cellular mechanism underlying its beneficial effects on systemic energy metabolism and lipid homeostasis.

NRF2 is a key transcription factor that controls the reaction of cells to oxidative stress.[34,35] Previous studies have indicated the intimate connection between oxidative stress and the development of metabolic syndrome, whereas cuproptosis itself can exacerbate oxidative damage.[8,36] The present study further emphasized how crucial the NRF2/ARE signaling pathway activation is in mediating the effects of EA. We propose that EA-induced NRF2 activation exerts

a dual function: first, by upregulating a series of antioxidant genes, it comprehensively enhances cellular antioxidant capacity and alleviates metabolic oxidative stress;[37,38] second, by indirectly modulating copper metabolism-related genes, it synergistically suppresses cuproptosis. The convergence of these two protective mechanisms may represent a key molecular pathway through which EA maintains metabolic homeostasis.

Our findings further extend the benefits of EA to the gut microbiome. EA intervention significantly reshaped the gut microbiota,[39] most notably by increasing the relative abundance of Limosilactobacillus and Ligilactobacillus. The probiotic strain Limosilactobacillus has a knack for prompting intestinal cells to crank out mucins and tight junction proteins like Occludin and ZO-1, which in turn fortifies the intestinal barrier. This reinforcement helps keep endotoxins and other nasty substances from slipping into the bloodstream, ultimately taking some of the heat off the liver by calming inflammation. Ligilactobacillus, in contrast, promotes mucin secretion, strengthens the intestinal barrier, regulates immune responses, and influences bile acid metabolism.[40–42] These microbial shifts were accompanied by a remodeling of the fecal metabolome, marked by elevated levels of metabolites such as L-cysteine, L-glutamic acid, succinate, and citrate.[43,44] These metabolites are functionally interconnected: L-cysteine serves as a precursor for GSH synthesis,[45] succinate and citrate are intermediates of the tricarboxylic acid cycle, and their altered levels reflect profound host–microbiota co-metabolic impacts on energy metabolism.[46,47] Additionally, L-glutamate is involved in nitrogen and energy metabolism.[48,49]

In light of these results, we suggest a theoretical working model wherein EA alters the activity of the central and autonomic nervous systems,[50] resulting in modifications to the intestinal environment (eg bile acid secretion and gut motility).[51] This shift favors the enrichment of advantageous bacteria, including Limosilactobacillus and Ligilactobacillus which in turn generate bioactive metabolites that enhance antioxidant defenses (eg L-cysteine) and regulate energy metabolism (eg succinate and citrate). Upon absorption, these metabolites systemically activate the NRF2 pathway and may directly or indirectly ameliorate MASLD progression in metabolic tissues, such as the liver,[52] collectively contributing to the observed improvements in serum lipid profiles and body weight.

Despite our promising results, this study has some limitations. First, although strong correlations were observed among EA intervention, microbiota metabolite changes, NRF2 activation, and cuproptosis inhibition, the causal relationships within this regulatory network require further experimental validation. Future studies employing approaches such as antibiotic-induced microbiota depletion[53] or fecal microbiota transplantation[54,55] will be valuable for clarifying the mechanistic contributions of gut microbes. Furthermore, employing NRF2-knockout models or cuproptosis-specific inhibitors in this context would be crucial to definitively establish the causal role of these pathways in mediating the therapeutic effects of EA. Second, the precise occurrence and spatial distribution of cuproptosis in the liver, as well as its modulation by EA, should be further confirmed using more specific detection techniques, such as Cu+-selective fluorescent probes.[56] While the present HFD model does not develop significant fibrosis, thereby precluding direct assessment of anti-fibrotic effects, our findings that EA alleviates oxidative stress and inflammation—the primary triggers of hepatic stellate cell activation—provide a crucial mechanistic basis for its potential to prevent fibrosis progression. Direct evaluation of EA's anti-fibrotic efficacy warrants future investigation in models of advanced MASLD.

Conclusion

This study demonstrates that the therapeutic effects of EA against MASLD are achieved through an integrated, multi-system mechanism. Specifically, EA alleviates hepatic steatosis, inflammation, and oxidative stress by activating the hepatic NRF2/ARE pathway. Importantly, this activation appears to serve as a central node in a coordinated regulatory network: by enhancing antioxidant capacity, EA not only reduces oxidative stress but also subsequently dampens the inflammatory response and mitigates mitochondrial dysfunction, thereby counteracting the process of cuproptosis. Concurrently, via modulation of the gut–liver axis, EA improves the gut microbiota composition and associated metabolite profiles, which may systemically support these hepatic improvements. Thus, EA likely disrupts the pathogenic cycle linking oxidative stress, inflammation, and cuproptosis, while also exerting beneficial effects on metabolic homeostasis, as shown in Figure 8. These findings provide a scientific basis for the application of EA as a multi-target therapeutic strategy for MASLD.

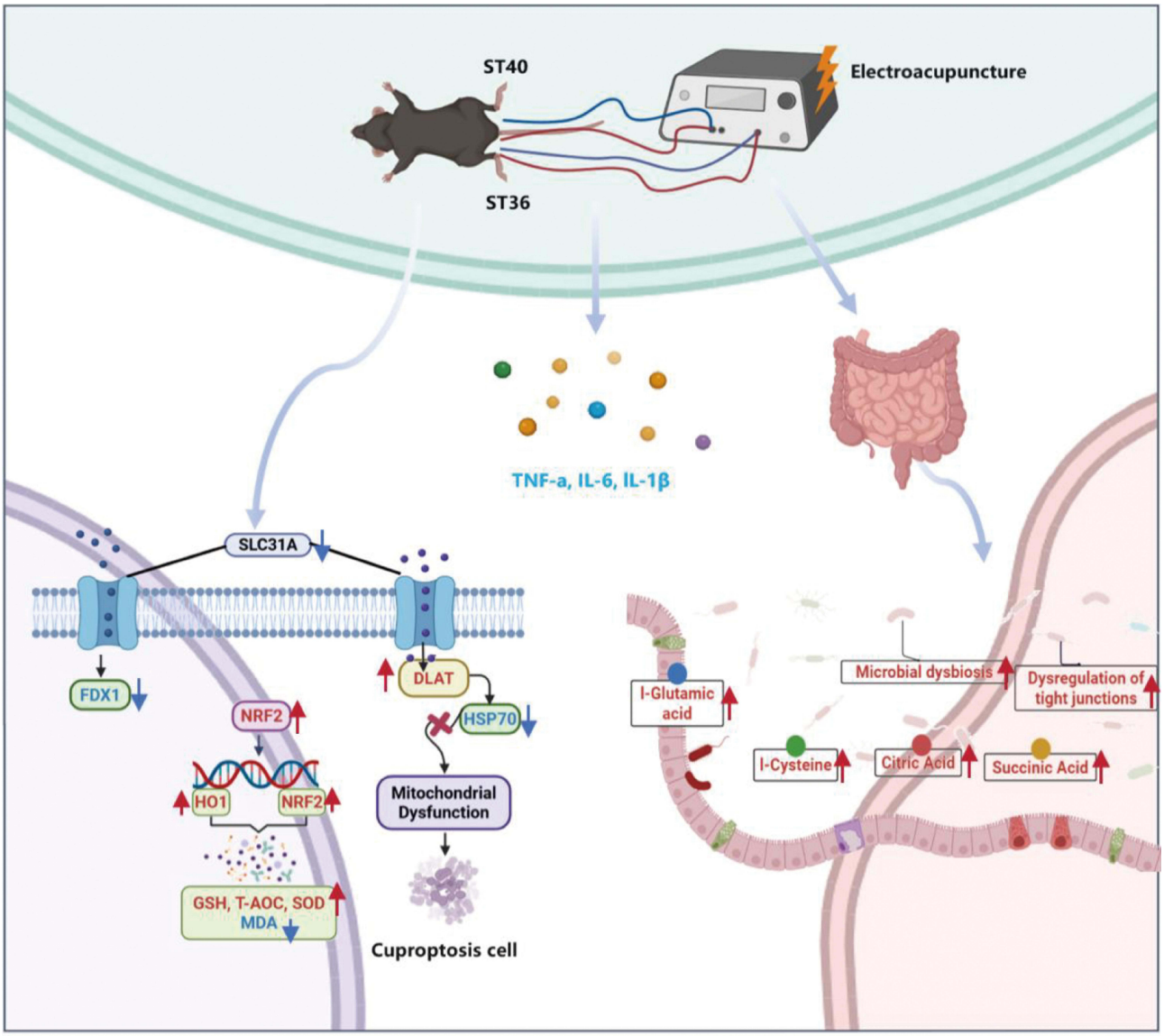

Figure 8 Schematic of the proposed mechanism.

Data Sharing Statement

The data generated in the present study may be obtained from the first author upon reasonable request.

Ethics Approval and Informed Consent

All procedures involving animals were approved by the Ethics Committee of Chongqing Medical University (IACUC-CQMU-2024-0215).

Acknowledgments

The authors gratefully acknowledge the professional English language editing services provided by Editage (www.editage.com), a brand of Cactus Communications, for improving the readability and language quality of this manuscript.

Author Contributions

Junyuan Deng: Writing – original draft, Conceptualization, Data curation. Cai Liao: Data curation, Writing – review & editing. Hejing Liu: Writing – original draft, Methodology. Xin Tang: Software, Writing – Review & Editing. Yan Yang:

Investigation, Writing – Review & Editing. Yunhao Yang: Formal analysis, Writing – Review & Editing. Xiao Guo: Data curation, Writing – Review & Editing. Shanshan Zhang: Investigation, Writing – Review & Editing. Kehan Xing: Validation, Writing – Review & Editing. Mei Liao: Validation, Writing – Review & Editing. Chenglin Tang: Writing – review & editing, Funding acquisition, Project administration. All authors made substantial contributions to the conception of the work, the acquisition, analysis, or interpretation of data, and drafting or critically revising the paper. All authors gave final approval of the version to be published and agree to be accountable for all aspects of the work. All authors have agreed on the journal to which the article will be submitted.

Funding

This research was funded by the National Natural Science Foundation of China (No.82405564), the General Program of Natural Science Foundation of Chongqing (Grant No.CSTB2023NSCQ-MSX0884), the Science and Technology Research Program of Chongqing Municipal Education Commission (Grant No.KJQN202315124), the Key Discipline Construction Project of Acupuncture Moxi-bustion and Massage of Chongqing Health Commission (472020320220021), College of Traditional Chinese Medicine of Chongqing Medical University (No: 2021-ZDXK-DB07) and Chongqing Yuzhong District Science and Technology Plan Project (No: 20200116).

Disclosure

The authors report no conflicts of interest.

References

1. Younossi ZM, Koenig AB, Abdelatif D, Fazel Y, Henry L, Wymer M. Global epidemiology of metabolic dysfunction-associated steatotic liver disease-meta-analytic assessment of prevalence, incidence, and outcomes. *Hepatology*. 2016;64(1):73–84. doi:10.1002/hep.28431
2. Riazi K, Azhari H, Charette JH, et al. The prevalence and incidence of MASLD worldwide: a systematic review and meta-analysis. *Lancet Gastroenterol Hepatol*. 2022;7(9):851–861. doi:10.1016/S2468-1253(22)00165-0
3. Diehl AM, Cause DC. Pathogenesis, and treatment of nonalcoholic steatohepatitis. *New Engl J Med*. 2017;377(21):2063–2072. doi:10.1056/NEJMra1503519
4. Adams LA, Lymp JF, St Sauver J, et al. The natural history of metabolic dysfunction-associated steatotic liver disease: a population-based cohort study. *Gastroenterology*. 2005;129(1):113–121. doi:10.1053/j.gastro.2005.04.014
5. Chalasani N, Younossi Z, Lavine JE, et al. The diagnosis and management of metabolic dysfunction-associated steatotic liver disease: practice guidance from the American Association for the Study of Liver Diseases. *Hepatology*. 2018;67(1):328–357. doi:10.1002/hep.29367
6. Tsvetkov P, Coy S, Petrova B, et al. Copper induces cell death by targeting lipoylated TCA cycle proteins. *Science*. 2022;375(6586):1254–1261. doi:10.1126/science.abf0529
7. Cobine PA, Brady DC. Cuproptosis: cellular and molecular mechanisms underlying copper-induced cell death. *Molecular Cell*. 2022;82(10):1786–1787. doi:10.1016/j.molcel.2022.05.001
8. Xie J, Yang Y, Gao Y, He J. Cuproptosis: mechanisms and links with cancers. *Mol Cancer*. 2023;22(1):46. doi:10.1186/s12943-023-01732-y
9. Jomova K, Valko M. Advances in metal-induced oxidative stress and human disease. *Toxicology*. 2011;283(2–3):65–87. doi:10.1016/j.tox.2011.03.001
10. Tan W, Zhang J, Chen L, et al. Copper homeostasis and cuproptosis-related genes: therapeutic perspectives in non-alcoholic fatty liver disease. *Diabetes Obesity Metab*. 2024;26(11):4830–4845. doi:10.1111/dom.15846
11. Tang D, Chen X, Kroemer G. Cuproptosis: a copper-triggered modality of mitochondrial cell death. *Cell Res*. 2022;32(5):417–418. doi:10.1038/s41422-022-00653-7
12. Tian Z, Jiang S, Zhou J, Zhang W. Copper homeostasis and cuproptosis in mitochondria. *Life Sci*. 2023;334:122223. doi:10.1016/j.lfs.2023.122223
13. Zhang R, Lao L, Ren K, Berman BM. Mechanisms of acupuncture-electroacupuncture on persistent pain. *Anesthesiology*. 2014;120(2):482–503. doi:10.1097/ALN.0000000000000101
14. Zhao ZQ. Neural mechanism underlying acupuncture analgesia. *Progress Neurobiol*. 2008;85(4):355–375. doi:10.1016/j.pneurobio.2008.05.004
15. Vilar-Gomez E, Martinez-Perez Y, Calzadilla-Bertot L, et al. Weight loss through lifestyle modification significantly reduces features of nonalcoholic steatohepatitis. *Gastroenterology*. 2015;149(2):367–378.e365;quize314–365. doi:10.1053/j.gastro.2015.04.005
16. Sanyal AJ, Chalasani N, Kowdley KV, et al. Pioglitazone, vitamin E, or placebo for nonalcoholic steatohepatitis. *New Engl J Med*. 2010;362(18):1675–1685. doi:10.1056/NEJMoa0907929
17. Bril F, Cusi K. Management of metabolic dysfunction-associated steatotic liver disease in patients with type 2 diabetes: a call to action. *Diabetes Care*. 2017;40(3):419–430. doi:10.2337/dc16-1787
18. Zhao J, Zhao X, Wang Q, et al. Efficacy and safety of electroacupuncture for metabolic dysfunction-associated fatty liver disease: a study protocol for a multicentre, randomised, sham acupuncture-controlled, patient-blinded clinical trial. *BMJ open*. 2024;14(11):e084768. doi:10.1136/bmjopen-2024-084768
19. Gao Y, Wang Y, Zhou J, Hu Z, Shi Y. Effectiveness of electroacupuncture for simple obesity: a systematic review and meta-analysis of randomized controlled trials. *Evid Based Complement Alternat Med*. 2020;2020:2367610. doi:10.1155/2020/2367610
20. Liu C, Ao Y, Liu B, et al. The safety and efficacy of acupuncture in treating metabolic dysfunction-associated steatotic liver disease: a systematic review and meta-analysis based on randomized controlled trials. *Medicine*. 2025;104(18):e42272. doi:10.1097/MD.0000000000042272
21. Steinberg GR, Valvano CM, De Nardo W, watt MJ. Integrative metabolism in MASLD and MASH: pathophysiology and emerging mechanisms. *J Hepatol*. 2025;83(2):584–595. doi:10.1016/j.jhep.2025.02.033

22. Hu XY, Luo Y, Zu F, et al. Effects of electroacupuncture at "Fenglong"(ST40) and "Zusanli"(ST36) on the SIRT1/FOXO1 signaling pathway in non-alcoholic fatty liver disease model rats. *Zhen ci yan jiu*. 2025;50(2):150–158. doi:10.13702/j.1000-0607.20240849
23. Liang W, Menke AL, Driessen A, et al. Establishment of a general NAFLD scoring system for rodent models and comparison to human liver pathology. *PLoS One*. 2014;9(12):e115922. doi:10.1371/journal.pone.0115922
24. Rinella ME. Metabolic dysfunction-associated steatotic liver disease: a systematic review. *JAMA*. 2015;313(22):2263–2273. doi:10.1001/jama.2015.5370
25. Cusi K, Orsak B, Bril F, et al. Long-term pioglitazone treatment for patients with nonalcoholic steatohepatitis and prediabetes or type 2 diabetes mellitus: a randomized trial. *Ann Internal Med*. 2016;165(5):305–315. doi:10.7326/M15-1774
26. Violi F, Cangemi R. Pioglitazone, vitamin E, or placebo for nonalcoholic steatohepatitis. *New Engl J Med*. 2010;363(12):1185–1186.
27. Athyros VG, Alexandrides TK, Bilianou H, et al. The use of statins alone, or in combination with pioglitazone and other drugs, for the treatment of non-alcoholic fatty liver disease/non-alcoholic steatohepatitis and related cardiovascular risk. *An Expert Panel Statement Metabol*. 2017;71:17–32.
28. Li YX, Xiao XL, Zhong DL, et al. Effectiveness and safety of acupuncture for migraine: an overview of systematic reviews. *Pain Res Manag*. 2020;2020:3825617. doi:10.1155/2020/3825617
29. Chen L, Min J, Wang F. Copper homeostasis and cuproptosis in health and disease. *Signal Transd Targeted Therapy*. 2022;7(1):378.
30. Wang W, Lu K, Jiang X, et al. Ferroptosis inducers enhanced cuproptosis induced by copper ionophores in primary liver cancer. *J Exp Clin Cancer Res*. 2023;42(1):142. doi:10.1186/s13046-023-02720-2
31. Huo S, Wang Q, Shi W, et al. ATF3/SPI1/SLC31A1 signaling promotes cuproptosis induced by advanced glycosylation end products in diabetic myocardial injury. *Int J Mol Sci*. 2023;24(2):1667. doi:10.3390/ijms24021667
32. Sun L, Zhang Y, Yang B, et al. Lactylation of METTL16 promotes cuproptosis via m(6)A-modification on FDX1 mRNA in gastric cancer. *Nat Commun*. 2023;14(1):6523.
33. Kahlson MA, Dixon SJ. Copper-induced cell death. *Science*. 2022;375(6586):1231–1232. doi:10.1126/science.abo3959
34. Tonelli C, Chio IIC, Tuveson DA. Transcriptional Regulation by Nrf2. *Antioxid Redox Signaling*. 2018;29(17):1727–1745. doi:10.1089/ars.2017.7342
35. Gorrini C, Baniasadi PS, Harris IS, et al. BRCA1 interacts with Nrf2 to regulate antioxidant signaling and cell survival. *J Exp Med*. 2013;210(8):1529–1544. doi:10.1084/jem.20121337
36. Masenga SK, Kabwe LS, Chakulya M, Kirabo A. Mechanisms of Oxidative Stress in Metabolic Syndrome. *Int J Mol Sci*. 2023;24(9):7898. doi:10.3390/ijms24097898
37. Ma Q. Role of nrf2 in oxidative stress and toxicity. *Ann Rev Pharmacol Toxicol*. 2013;53:401–426. doi:10.1146/annurev-pharmtox-011112-140320
38. Bellezza I, Giambanco I, Minelli A, Donato R. Nrf2-Keap1 signaling in oxidative and reductive stress. *Biochim Biophys Acta Mol Cel Res*. 2018;1865(5):721–733. doi:10.1016/j.bbamcr.2018.02.010
39. Yang Y, Pang F, Zhou M, et al. Electroacupuncture reduces inflammatory bowel disease in obese mice by activating the Nrf2/HO-1 signaling pathways and repairing the intestinal barrier. *Diabetes Metabolic Syndrome and Obesity*. 2024;17:435–452. doi:10.2147/DMSO.S449112
40. Yue N, Zhao H, Hu P, et al. Real-world of Limosilactobacillus reuteri in mitigation of acute experimental colitis. *J Nanobiotechnol*. 2025;23(1):65. doi:10.1186/s12951-025-03158-8
41. Yi W, Shi J, Wang L, et al. Maternal PFOS exposure in mice induces hepatic lipid accumulation and inflammation in adult female offspring: involvement of microbiome-gut-liver axis and autophagy. *J Hazard Mater*. 2024;470:134177. doi:10.1016/j.jhazmat.2024.134177
42. Gao J, He Y, Shi F, et al. Activation of Sirt6 by icariside II alleviates depressive behaviors in mice with poststroke depression by modulating microbiota-gut-brain axis. *J Adv Res*. 2025.
43. Koh A, De Vadder F, Kovatcheva-Datchary P, Bäckhed F. From dietary fiber to host physiology: short-chain fatty acids as key bacterial metabolites. *Cell*. 2016;165(6):1332–1345. doi:10.1016/j.cell.2016.05.041
44. Krautkramer KA, Fan J, Bäckhed F. Gut microbial metabolites as multi-kingdom intermediates. *Nat Rev Microbiol*. 2021;19(2):77–94. doi:10.1038/s41579-020-0438-4
45. Forman HJ, Zhang H, Rinna A. Glutathione: overview of its protective roles, measurement, and biosynthesis. *Mol Aspect Med*. 2009;30(1–2):1–12. doi:10.1016/j.mam.2008.08.006
46. Mills E, O'Neill LA. Succinate: a metabolic signal in inflammation. *Trends Cell Biol*. 2014;24(5):313–320. doi:10.1016/j.tcb.2013.11.008
47. Du L, Li Q, Yi H, Kuang T, Tang Y, Fan G. Gut microbiota-derived metabolites as key actors in type 2 diabetes mellitus. *Biomed Pharmacothe*. 2022;149:112839. doi:10.1016/j.biopha.2022.112839
48. Newsholme P, Procopio J, Lima MM, Pithon-Curi TC, Curi R. Glutamine and glutamate--their central role in cell metabolism and function. *Cell Biochem Funct*. 2003;21(1):1–9. doi:10.1002/cbf.1003
49. Kondoh T, Mallick HN, Torii K. Activation of the gut-brain axis by dietary glutamate and physiologic significance in energy homeostasis. *Ame J Clin Nutrit*. 2009;90(3):832s–837s. doi:10.3945/ajcn.2009.27462V
50. Carabotti M, Scirocco A, Maselli MA, Severi C. The gut-brain axis: interactions between enteric microbiota, central and enteric nervous systems. *Ann gastroenterol*. 2015;28(2):203–209.
51. Sayin SI, Wahlström A, Felin J, et al. Gut microbiota regulates bile acid metabolism by reducing the levels of tauro-beta-muricholic acid, a naturally occurring FXR antagonist. *Cell Metab*. 2013;17(2):225–235. doi:10.1016/j.cmet.2013.01.003
52. Hayes JD, Dinkova-Kostova AT. The Nrf2 regulatory network provides an interface between redox and intermediary metabolism. *Trends Biochem Sci*. 2014;39(4):199–218. doi:10.1016/j.tibs.2014.02.002
53. Reikvam DH, Erofeev A, Sandvik A, et al. Depletion of murine intestinal microbiota: effects on gut mucosa and epithelial gene expression. *PLoS One*. 2011;6(3):e17996. doi:10.1371/journal.pone.0017996
54. Xue L, Deng Z, Luo W, He X, Chen Y. Effect of fecal microbiota transplantation on non-alcoholic fatty liver disease: a randomized clinical trial. *Front Cell Infect Microbiol*. 2022;12:759306. doi:10.3389/fcimb.2022.759306
55. Wang J, Chen J, Chen M. Commentary: effect of fecal microbiota transplantation on non-alcoholic fatty liver disease: a randomized clinical trial. *Front Cell Infect Microbiol*. 2022;12:1056394. doi:10.3389/fcimb.2022.1056394
56. Zeng X, Gao S, Jiang C, et al. Rhodol-derived turn-on fluorescent probe for copper ions with high selectivity and sensitivity. *Luminescence*. 2021;36(7):1761–1766. doi:10.1002/bio.4118